

Clustering and descendants of MUSYC galaxies at $z < 1.5$

Padilla, N.D.¹, Christlein, D.², Gawiser, E.³, González, R.E.¹, Guaita, L.¹, Infante, L.¹.

¹ *Departamento de Astronomía y Astrofísica, Pontificia Universidad Católica de Chile, V. Mackenna 4860, Santiago 22, Chile.*

² *Max Planck Institut für Astrophysik, Garching, Germany*

³ *Astronomy Department, Rutgers University, USA.*

13 November 2018

ABSTRACT

We measure the evolution of galaxy clustering out to a redshift of $z \simeq 1.5$ using data from two MUSYC fields, the Extended Hubble Deep Field South (EHDF-S) and the Extended Chandra Deep Field South (ECDF-S). We use photometric redshift information to calculate the projected-angular correlation function, $\omega(\sigma)$, from which we infer the projected correlation function $\Xi(\sigma)$. We demonstrate that this technique delivers accurate measurements of clustering even when large redshift measurement errors affect the data. To this aim we use two mock MUSYC fields extracted from a Λ CDM simulation populated with GALFORM semi-analytic galaxies which allow us to assess the degree of accuracy of our estimates of $\Xi(\sigma)$ and to identify and correct for systematic effects in our measurements. We study the evolution of clustering for volume limited subsamples of galaxies selected using their photometric redshifts and rest-frame r -band absolute magnitudes. We find that the real-space correlation length r_0 of bright galaxies, $M_r < -21$ (rest-frame) can be accurately recovered out to $z \simeq 1.5$, particularly for ECDF-S given its near-infrared photometric coverage. For these samples, the correlation length is consistent with a constant value of $r_0 = (2.6 \pm 0.3)h^{-1}\text{Mpc}$ for the ECDF-S field, and $r_0 = (3.0 \pm 0.4)h^{-1}\text{Mpc}$ for the EHDF-S field from a median redshift $z_{\text{med}} = 0.37$ to $z_{\text{med}} = 1.15$. There is mild evidence for a luminosity dependent clustering in both fields at the low redshift samples (up to $z < 0.57$), where the correlation length is higher for brighter galaxies by up to $1\text{Mpc}/h$ between median rest-frame r -band absolute magnitudes of ~ -18 to ~ -21.5 . As a result of the photometric redshift measurement, each galaxy is assigned a best-fit template; we restrict to E and E+20%Sbc types to construct subsamples of early type galaxies (ETGs). These ETGs are separated into samples at different redshift intervals so that their passively evolved luminosities (to $z = 0$) are comparable. Our ETG samples show a strong increase in r_0 as the redshift increases, making it unlikely (95% level) that ETGs at median redshift $z_{\text{med}} = 1.15$ are the direct progenitors of ETGs at $z_{\text{med}} = 0.37$ with equivalent passively evolved luminosities.

Key words: galaxies: distances and redshifts, galaxies: statistics, cosmology: observations, large-scale structure of the Universe.

1 INTRODUCTION

The evolution of galaxy clustering with redshift is a critical test of the paradigm of galaxy and structure formation favoured today. Large galaxy redshift surveys such as the 2dF Galaxy Redshift Survey (2dFGRS, Colless et al. 2001) and the Sloan Digital Sky Survey (SDSS, York et al. 2000), have mapped the local galaxy population. Along with recent measurements from the cosmic microwave background radiation by WMAP, they have constrained with unprecedented accuracy several cosmological parameters (Dunkley

et al., 2009; Spergel et al., 2007; Sánchez et al., 2006). The study of the evolution of galaxy clustering with redshift can allow us to provide further tests to galaxy formation models by probing the evolution of the amplitude of fluctuations in the quasi-linear to non-linear regime, which only recently is becoming better understood by means of large numerical simulations (Colberg et al. 2000; Sheth, Mo & Tormen, 2001; Padilla & Baugh, 2002; Slejak & Warren, 2004). On the other hand, studies on the evolution of clustering will also allow to probe the evolution of the relation between galaxies

and the underlying dark matter, which is often parametrised by the bias parameter (e.g. Coil et al., 2004; Le Fèvre et al., 2005; Ouchi et al., 2004).

It is now becoming possible to perform deep galaxy redshift surveys, such as the DEEP2 Galaxy redshift survey (Coil et al., 2004), the VIMOS VLT Deep Survey (VVDS, Le Fèvre et al. 2005), and the zCOSMOS redshift survey (Meneux et al., 2009) which allow the study of the evolution of clustering with redshift. Coil et al. (2004) obtained the evolution of the correlation length using 2,220 DEEP2 galaxies, Le Fèvre et al. (2005) using $\sim 10,000$ VVDS galaxies, and Meneux et al. (2009) using a similar number of zCOSMOS galaxies. These studies, however, only reach redshifts of about $z = 1$, mainly due to the selection of galaxies by setting a lower limit on the photometric flux, which preferentially selects galaxies at relatively moderate redshifts, and are affected by cosmic variance due to the relatively small surveyed volumes.

There are several techniques that take advantage of features in the spectral energy distribution (SED) to identify sets of galaxies at a particular redshift range. These techniques use the Lyman Break in the SED at $z \sim 4$ and $z \sim 3$ (Ouchi et al., 2004; Lee et al., 2006; Adelberger et al., 2005a, 2005b), or identify galaxies with a Lyman- α line in emission at $z = 2.1, 3.1, 4.5, 4.86$ (Guaita et al., 2010, Gronwall et al., 2007, and Gawiser et al., 2007; Kovac et al., 2007; Ouchi et al., 2003, respectively), with the H α line in emission (e.g. Sobral et al., 2010), or use faint sources selected in the K-band (e.g. Quadri et al., 2007). Measurements of clustering from such samples, however, are somewhat hindered by the relatively low numbers of galaxies. A recent measurement of the clustering of galaxies selected using the Lyman- α emission (LAE galaxies) technique was performed by Gawiser et al. (2007). They point out that different samples of galaxies at high redshift, such as Lyman Break Galaxies and LAEs trace different underlying galaxy populations that can be related via their clustering measurements with the aid of a theoretical framework. Gawiser et al. first provide a thorough comparison between different available clustering measurements from $z = 0$ to $z \simeq 5$, and then analyse whether samples at different redshifts can be considered to be related in a parent/descendant relationship (see also Quadri et al., 2007, Francke et al., 2008, Guaita et al., 2010). The latter is achieved by comparing their measured clustering with expected trends of the bias parameter with redshift extracted from simple analytic approximations in a Λ CDM model. This allows them to connect the LAE population at $z = 3.1$ to present-day L^* galaxies.

Another interesting approach is that presented by Zheng, Coil & Zehavi (2007, see also White et al., 2007, Brown et al., 2008, Wake et al., 2008), who fit the projected correlation functions measured in SDSS and DEEP2 using the Halo Occupation Distribution model (HOD, see for example Jing, Mo & Börner, 1998, Peacock & Smith, 2000, Cooray & Sheth, 2002). Using this powerful technique Zheng et al. are able to determine that the rate of growth of the stellar mass is smaller in central than in satellite galaxies between redshifts ~ 1 and ~ 0 , and the fraction of stellar mass in satellites diminishes at high redshifts. An interesting prospect is that of putting together theoretical models for the evolution of haloes with HODs and applying the analysis to large sets of measurements of high- z galaxies.

Within this picture, intermediate redshift surveys such as DEEP2 and VVDS, which cover the range $0.3 < z < 1.0$, bridge the gap between the low redshift surveys such as SDSS and 2dFGRS, and the samples of LAEs, LBGs and other photometrically selected galaxies at high redshifts. In this paper we will analyse the clustering of volume limited samples of MUSYC galaxies¹, to complement this intermediate redshift range, studying galaxy populations of various luminosities and redshifts out to $z = 1.5$.

The detailed evolution of the galaxy clustering can also be used to study the assembly of passive galaxies. This particular subject has recently become the centrepiece of a discussion regarding galaxy evolution. It has been claimed that high stellar mass, passive galaxies do not show an evolution in their comoving space density. This has been studied using the stellar mass and luminosity functions in observations (Cimatti et al., 2002, 2004; McCarthy et al., 2004; Glazebrook et al. 2004; Daddi et al., 2005; Saracco et al., 2005; Pérez-González et al., 2008; Bundy et al., 2006), and has been interpreted as evidence that their stellar content has already been assembled at high redshift, ruling out the involvement of (even dry) mergers in the build up of their stellar mass. Results from models of galaxy formation indicate that massive galaxies would continue to acquire stellar mass at comparatively lower redshifts (e.g. De Lucia et al., 2006, Lagos, Cora & Padilla, 2008, Lagos, Padilla & Cora, 2009). Measurements of clustering offer an alternative way to assess this problem which consists of connecting a population of galaxies at high redshift to a low redshift population, via the expected evolution of clustering. In this work we will test this approach using our MUSYC sample.

This paper is organised as follows. We describe the MUSYC data in Section 2; Section 3 describes the numerical simulation, the procedure followed to construct the mock catalogues, and their role in our analysis. The method used to infer the clustering measurement is described in Section 4 and thoroughly tested in Section 5, and the results from the MUSYC galaxies are presented in Section 6. We discuss our results in Section 7 and present our main conclusions in Section 8.

2 MUSYC

The Multi-wavelength Survey by Yale-Chile (MUSYC) comprises 1.2 square degrees of sky. The full survey covers four fields chosen to leverage existing data and to enable flexible scheduling of observing time during the year. Each field is imaged from the ground in the optical and near-infrared. Follow-up spectroscopy is done mostly with multi-object spectrographs (VIMOS and IMACS). The survey fields will be a natural choice for future observations with ALMA. The data used in this paper corresponds to two MUSYC fields with the most complete photometric and spectroscopic coverage, the EHDF-S and ECDF-S fields. These fields include imaging in the U, B, V, R filters to AB depths of 26.5 plus additional shallower imaging in I and z . The $ECDF-S$ field also includes K, J imaging to a depth of 22.5 AB. Both fields

¹ For full details on the survey see the MUSYC collaboration web-page <http://www.astro.yale.edu/MUSYC>.

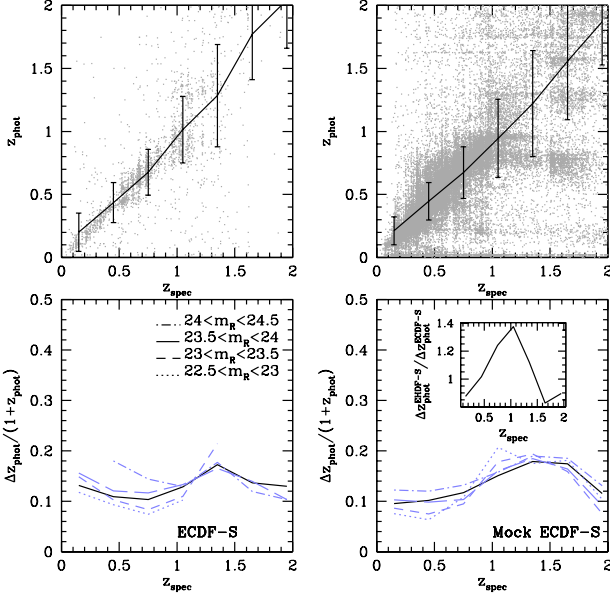


Figure 1. Photo- z vs. Spectroscopic redshifts for the ECDF-S field (top-left) and a mock catalogue (top-right). The lower panels indicate the relative error in redshift, as a function of the intrinsic galaxy luminosity (absolute magnitude ranges are indicated in the key). The inset on the lower right panel shows the ratio between the photo- z errors obtained from mock catalogues with the photometry available in the EHDF-S and the ECDF-S (the former does not include infra-red photometry).

include extensive follow-up spectroscopy of specific colour-selected galaxy samples.

In MUSYC, galaxies are defined as sources identified using SExtractor (Bertin & Arnouts, 1996) on the co-added BVR images, with SExtractor stellarity parameter $c < 0.8$ (Huber, 2002²). The total number of galaxies in MUSYC is $\sim 280,000$ at $m_{BVR} < 27.1$; after restricting our samples, this number decreases to $\sim 50,000$ galaxies.

Photometric redshifts were estimated using a least squares frequentist best-fit (e.g. Bayarri & Berger, 2004) to the observed photometry of MUSYC galaxies. The templates in the synthetic set adopted by HYPERZ (Bolzonella, Miralles & Pelló, 2000), allowed to evolve with time, are used to represent the redshift/spectral type mix in MUSYC. Once a photometric redshift and a best fitting evolving template are assigned to a galaxy, the latter is compared to a collection of 11 templates selected as in Christlein et al. (2009). The Christlein et al. templates correspond to different $z = 0$ galaxy morphologies from early types (E, E+20%Sbc) to late type Irr galaxies, and allow us to define a galaxy morphology from the best fitting evolving template. When calculating the redshift probabilities, we used all available MUSYC flux measurements from all the available bands. As can be seen in the top-left panel of Figure 1, the resulting photometric redshifts out to $z_{spec} \simeq 1.5$ agree to roughly 30%

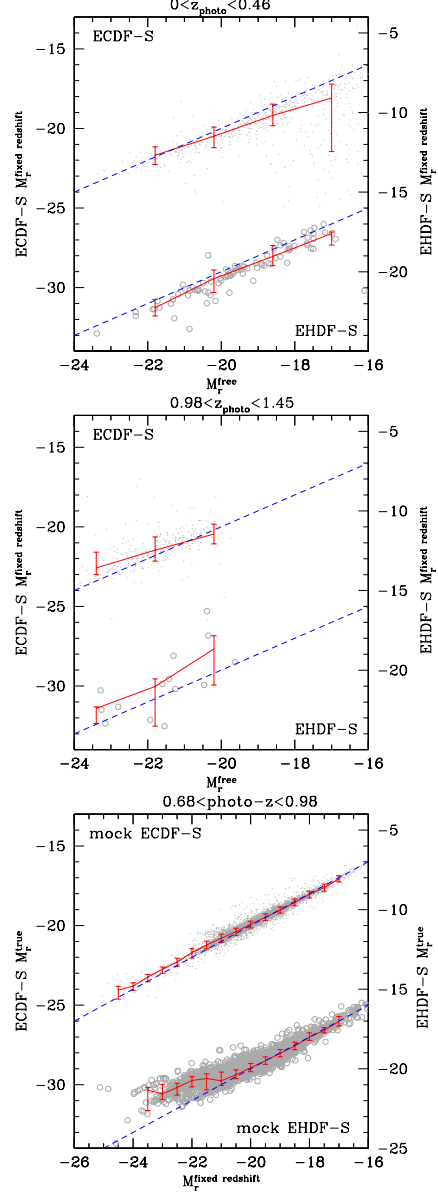


Figure 2. Top and Middle panels: Recovered (M_{free}) vs. true ($M_{fixedredshift}$) absolute magnitudes in the r band for galaxies in the ECDF-S (dots, upper line) and EHDF-S (open circles, lower line) fields. Each panel shows a different redshift slice, indicated on the top. The left-hand (right-hand) y-axis shows the M_r scale for the ECDF-S (EHDF-S). The lines with errorbars show the median and 10 and 90 percentiles, respectively. The dashed lines show the one-to-one relation. Bottom panel: recovery of the true rest-frame r -band absolute magnitude in the Bower et al. mocks, when fixing the redshift at its spectroscopic value. Lines and symbols are as in the top two panels.

with the spectroscopic redshifts. This analysis arises from a sample of 3193 galaxies with available spectroscopic redshift measurements in the ECDF-S from available MUSYC spectroscopy and the NED database. The lower-left panel shows in different line types different limits in R -band apparent magnitudes, and indicates that photometric redshift (photo- z) errors change only slightly with galaxy luminosity. The lack of severe degeneracies is also clear in our photo- z

² Huber (2002) estimate a SExtractor stellarity parameter $c = 0.8$ as the most adequate value for separating stars ($c > 0.8$) and galaxies. Our results do not change significantly when varying the stellarity threshold from 0.75 to 0.85.

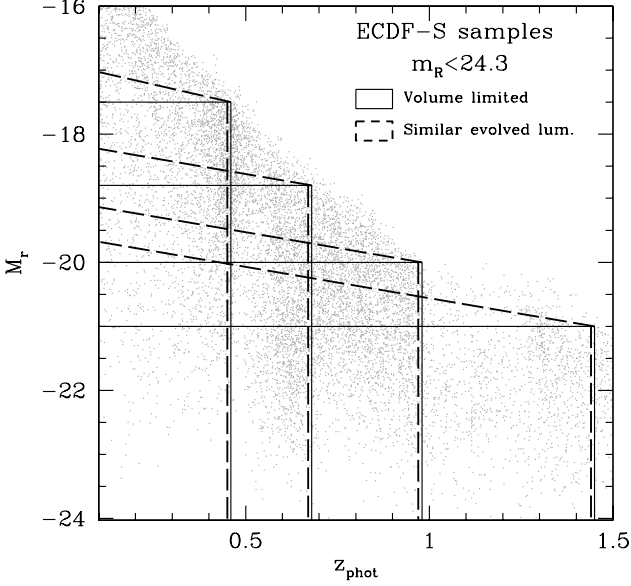


Figure 3. Construction of centre galaxy samples for our cross-correlation measurements. The points represent galaxies in the ECDF-S field with apparent magnitudes below the completeness limit, $m_R < 24.3$. The vertical lines show the adopted limits in redshift. Horizontal lines show different limits in rest-frame absolute magnitudes M_r used as further constraints in the construction of galaxy samples. The long-dashed lines show the limiting luminosities adopted for samples of early-type galaxies selected so as to have similar passively evolved luminosities at different redshifts.

estimates. This comparison indicates that the error in the estimate of photometric redshifts is $\Delta z = 0.09(1 + z)$ after removing $5-\sigma$ outliers (The normalised median absolute deviation, NMAD, calculated according to Hoaglin et al., 1983, is 0.065). The removal of outliers diminishes the sample of ECDF-S galaxies by a 10%. We do not use galaxies fainter than $m_R = 24.3$ since at these apparent magnitudes the quality of the photometric redshift estimation starts to degrade. The dots in the figure represent each galaxy in the ECDF-S down to this magnitude limit. For EHDF-S the total number of spectroscopic redshifts available amounts to 405 (much less than for ECDF-S). The comparison between spectroscopic and photometric redshifts shows that photo- z errors are consistent with those for ECDF-S, even when there is no near-infrared photometry for this field. The removal of the $5-\sigma$ outliers diminishes the EHDF-S sample by a 16%. As will be shown in Section 3, the analysis of mock catalogues with the photometry available in the EHDF-S and ECDF-S suggests that the photo- z errors in the former will be up to a factor 1.4 higher (see the inset in the lower-right panel of the figure), as a result of the lack of infra-red photometry in this field. This also increases the amount of catastrophic errors in EHDF-S; the mock catalogues will allow us to assess the degree out to which this will affect the EHDF-S results.

The upper and middle panels of Figure 2 show the comparison between the rest-frame r-band absolute magnitudes (M_r) estimated using the spectroscopic and photometric redshifts of each galaxy, for the EHDF-S and ECDF-S fields, for two different redshift slices (indicated in each panel). In

all cases, the photo- z estimates of M_r show offsets of up to ~ 1 magnitude from the spectroscopic ones. In the case of EHDF-S, at $z_{\text{photo}} > 0.98$, this difference may be higher, of up to ~ 2 mags, but the low number of spectroscopic redshifts available does not allow to reach a firm conclusion on this regard; however, the analysis of mock catalogues will confirm that the recovery of M_r is expected to be significantly better in ECDF-S (see the lower panel).

In our clustering measurements we will use two types of galaxy samples. Centre samples around which the clustering will be measured, and tracer samples that will be used to trace the structure around each centre galaxy. We restrict centre galaxies to the redshift range $0.1 < z_{\text{photo}} < 1.45$ and divide the data in four “centre” subsamples, defined by photo- z ranges limited by $0.1 - 0.46$, $0.46 - 0.68$, $0.68 - 0.98$ and $0.98 - 1.45$; these limits are set so as to probe a wide redshift range. The resulting median photometric redshifts are $z = 0.38, 0.46, 0.81$ and 1.14 , and the sampled volumes are approximately $80,000h^{-3}\text{Mpc}^3$, $129,000h^{-3}\text{Mpc}^3$, $262,000h^{-3}\text{Mpc}^3$, and $550,000h^{-3}\text{Mpc}^3$ for the lower to higher redshift samples, respectively. The aim in dividing the sample in different bins of redshift is to be able to detect a variation in the clustering of galaxies with redshift. Additionally, we apply rest-frame r-band absolute magnitude cuts to construct volume limited samples; these are illustrated by the solid lines in Figure 3. Since we will use a cross-correlation technique, we define samples of tracer galaxies, which are galaxies selected using the same absolute magnitude cuts, but allowing a further $\delta z = 0.1$ to each side of the corresponding redshift interval (with the restriction of maximum redshift $z = 1.5$). This has the advantage of improving the statistical signal while only inducing small correlations between results from different redshift slices since the centre samples do not overlap (we do expect correlations arising from the photo- z errors which will contaminate neighbour redshift bins, and also from fluctuations of large-scale modes straddling the centre samples).

We also construct samples of early-type galaxies with similar passively evolved luminosities. In order to select ETGs, we find the $z = 0$ template that best matches the evolving template that was originally fit to the galaxy in the photo- z calculation. This effectively selects ETGs with similar colours at different redshifts. In order to select similar passively evolved luminosities, we use the empirical passive evolution recipe adopted by Cimatti et al. (2006) for the B-band, where

$$M_B(z=0) = M_B^{rf}(z) + 1.15 \times z, \quad (1)$$

where $M_B(z=0)$ is the absolute magnitude of a galaxy passively evolved to $z=0$; at redshift z the galaxy has a rest-frame absolute magnitude M_B^{rf} . This recipe is derived empirically from the evolution of the Fundamental Plane for massive early-type galaxies (di Serego Alighieri et al., 2005). As our samples are characterised by r-band magnitudes we find the corresponding evolution recipe in the r-band using models for the spectra of early-type galaxies (ETGs) approximated by single stellar populations (SSP). We first look for the SSP that best matches the evolution recipe from Eq. 1 using spectral energy distributions (SED) constructed using Bruzual & Charlot (2003, BC03) stellar synthesis algorithm and the Padova 2000 evolutionary tracks with a Salpeter initial mass function and a metallicity $[Fe/H] = 0.3$ - this

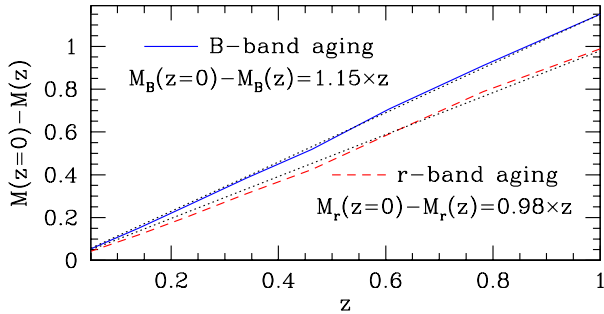


Figure 4. Variation in the absolute magnitude of a SSP (3.5Gyr old at $z = 1$) as a function of redshift, in the B- and r-band (solid and dashed lines, respectively). The dotted lines correspond to the fits indicated in the figure key. The upper line shows the recipe adopted by Cimatti et al. for the B-band, the lower dotted line shows the best fit to the evolution of the SSP in the r-band.

particular metallicity is adequate for high mass ETGs (e.g. Gallazzi et al., 2006). We find that a SSP which at $z = 1$ is 3.5Gyr old provides the best match to the recipe of Eq. 1 (consistent with studies by Bell et al., 2004). This can be seen in Figure 4 which shows the evolution of the B-band magnitude for this SED along with the recipe from Eq. 1. The figure also shows the evolution of the r-band magnitude for the same SEDs along with the best fit to the r-band evolution which corresponds to

$$M_r(z=0) = M_r^f + 0.98 \times z, \quad (2)$$

where M_r^f is the rest-frame luminosity at redshift z . We use the relation from Eq. 2 to construct samples with comparable evolved $z = 0$ r-band luminosities delimited by $M_r(z=0) = -16.85, -18.2, -19$, and -19.6 . We notice that the evolution recipe adopted here is particularly adequate for massive ETGs (di Serego Alighieri et al., 2005); even though we apply it to faint galaxies as well, we will only make comparisons between different redshift bins for the brightest samples. We apply the same redshift cuts used in the construction of the volume limited samples (see above). The resulting samples are illustrated in Figure 3 by the dashed lines (the vertical lines have been slightly displaced to improve clarity); the dependence of M_r on redshift shown by these lines correspond to the evolution of the ETG SED from Eq. 2, and as can be seen, the ETG samples selected this way should be complete since the dependence of the selection effect is stronger than the modeled passive evolution. Given that the detection of sources is done using optical filters (B,V and R), it could be possible that this will act against a complete selection of ETGs as proposed here. However, the detection limit in the combined optical photometry is 2.8 magnitudes deeper in flux than the sample selection cut. Still, in order to check whether this is affecting our results, we will also use the available imaging in the K band to produce an alternative sample of ETGs for the ECDF-S (this is not available for EHDF-S); the equivalent magnitude limit that produces a sample of ETGs comparable the one obtained in the R-band is $m_{K,lim} = 22.5$.

We note that our samples of ETGs will consist of read-and-dead galaxies at all the redshift intervals chosen. As we will show in Section 6, our approach is consistent with selecting galaxies in the red branch of the bimodal colour dis-

tribution, that is, in the red sequence. The latter has been widely used to study ETG properties and clustering evolution, as in Bell et al. (2004), Faber et al. (2006), and Coil et al. (2008). Another possibility for the selection of ETG samples in a direct descendant line at different redshifts is to let the colour of the galaxy templates evolve, but in this case we find that the selected galaxies either include blue cloud objects in our higher redshift samples or too few objects at low redshifts, mainly due to the small solid angle of the MUSYC survey. This can be taken as a possible indication that the samples of ETGs constructed by selecting galaxies in the red sequence with similar $z = 0$ passively evolved luminosities, may not constitute the parents and descendants of one another. However, small amounts of star-formation could easily change the colours of ETGs, making this comparison difficult. In order to overcome this problem, from this point on we will only analyse the possible parent/descendant relationship between ETG MUSYC samples at a given redshift and SDSS ETG samples at $z = 0$.

As over the individual redshift ranges probed by our analysis the change in clustering amplitude is expected to be roughly linear with redshift, our clustering measurements will be quoted at the median redshift of the galaxy subsample.

3 MOCK CATALOGUES

Due to the large uncertainties in the determination of photometric redshifts it is necessary to assess the effects arising from possible sources of systematics in our procedure. In order to do this, we use two mock catalogues extracted from a Λ CDM numerical simulation populated with GALFORM (versions corresponding to Baugh et al., 2005, and Bower et al., 2006) semi-analytic galaxies, kindly provided by the Durham group. As the underlying clustering and its evolution in the simulation are known, the results from the mock catalogues can be used to find systematic biases in our estimates, and to devise a method to account for them using only data available in the observational sample. The clustering of galaxies in the simulation mimics reasonably well the clustering of real galaxies, which makes the use of these mocks appropriate to test our method.

We construct two of mock catalogues, one of them using a single $z = 0$ simulation output (and therefore with a constant clustering with redshift) with Baugh et al. (2005) galaxies. The other mock is constructed using simulation outputs at different redshifts (i.e. an evolving lightcone) containing Bower et al. (2006) galaxies; this mock catalogue includes the evolution of the galaxy population and their clustering with redshift as results from the adopted cosmology and the assumptions in the semi-analytic galaxy formation model of Bower et al. In both cases, subsamples of different rest-frame luminosities show different clustering strengths. The ability of our measurement method to detect these variations will allow a study of the reliability of any clustering dependence on luminosity and redshift found in the real data.

There are a total of 10^9 particles in this simulation, the box side measures $1000h^{-1}\text{Mpc}$ a side, the matter density parameter corresponds to $\Omega_m = 0.25$, the value of the dark energy density parameter is $\Omega_\Lambda = 0.75$, the Hubble constant,

$H = 100h\text{kms}^{-1}\text{Mpc}^{-1}$, with $h = 0.7$, and the primordial power spectrum slope, $n_s = 0.97$. The present day amplitude of fluctuations in spheres of $8h^{-1}\text{Mpc}$ is set to $\sigma_8 = 0.8$. This particular cosmology is in line with recent cosmic microwave background anisotropy and large scale structure measurements (WMAP team, Dunkley et al., 2009, Spergel et al. 2007, Sánchez et al., 2006). We have adopted this cosmology for all the calculations performed throughout this paper.

The mock catalogues are constructed by selecting a suitable direction in the simulation cube and following it out to $z = 3$ replicating the simulation as many times as needed (4 in total, including outputs at different redshifts in the Bower et al. case). The direction is selected such that the structures sampled by the cone are not repeated. The estimates of uncertainties will be obtained using the jackknife technique applied to each mock field individually. This technique has been shown to provide uncertainties comparable to the scatter in clustering results from large numbers of individual mock catalogues (see for instance, Padilla et al., 2001).

The process of assigning galaxies to the mock catalogues consists of checking that the angular position of the galaxy falls within the MUSYC angular mask, and by placing the same apparent and absolute magnitude limit cuts as in the MUSYC data defined in Section 2. These magnitude limit cuts imprint a radial selection function in the mock catalogues which is qualitatively similar to that of the real data (obtained using photo-zs).

We apply the least squares frequentist best-fit method to assign photometric redshifts to mock galaxies, replicating the process followed for the observational data as well as the available photometry (i.e. different mocks for EHDF-S and ECDF-S galaxies). A comparison between underlying (spectroscopic) and photometrically derived redshifts for a Bower et al. ECDF-S mock is shown in the right panels of Figure 1; the lower right panel shows that the photo-z redshift uncertainties are comparable to those present in the real data (left panels). Additionally, the top-right panel shows a similar pattern as the MUSYC galaxies, with structures in the scatter plot situated at particular values of spectroscopic redshift reflecting the large-scale structure, and at certain values of photometric redshift due to attractors in the photometric fitting solution. This comparison further ensures us we have a proper tool to determine the statistical and systematic errors in the measured clustering amplitude arising from realistic photo-z errors. We calculate the photo-z errors for a Bower et al. EHDF-S mock, and perform the ratio between these errors and those obtained for the ECDF-S mock. This ratio is shown in the inset of the lower-right panel of Figure 1 where it can be seen that the lack of near infrared data in EHDF-S results in photo-z errors of up to a factor 1.4 larger than in the ECDF-S mock.

Using the mocks, we also test whether the adopted template set allows us to recover the true rest-frame absolute magnitude in the r-band from the available photometry. To do this we apply the template fitting procedure fixing the redshift at its spectroscopic (true) value. The comparison indicates that for the ECDF-S photometry the recovery is very precise, with systematic offsets lower than 0.2 magnitudes. The EHDF-S shows a good recovery for galaxies of all luminosities at $z < 0.45$; at higher redshifts this is true only for faint galaxies with $M_r > -21.5$. Brighter galaxies show

inferred magnitudes systematically brighter by ~ 1.5 mags, as can be seen in the example shown in the bottom panel of Figure 2. Such an offset was expected to some degree since the available photometry in EHDF-S, UBVRIz, only allows to obtain an extrapolated rest-frame r-band magnitude at redshifts $z > 0.5$. We will bear in mind this possible systematic offset when analysing the EHDF-S results at this redshift range.

4 METHOD

Our aim is to obtain a reliable measurement of the real-space correlation length r_0 , the separation at which the 3D spatial correlation function satisfies $\xi(r_0) = 1$. In the following description we will use the term “redshift” to refer to photo-zs in the case of MUSYC data, and to refer to either photometric or spectroscopic redshifts in the case of the mock catalogues (in this case, spectroscopic redshifts correspond to the true galaxy redshifts); when analysing the latter, spectroscopic redshifts will be used to infer the true underlying clustering present in the mock samples. We will apply the following steps both to real and mock data:

(i) Measure the projected-angular cross-correlation function $\omega(\sigma)$ as a function of the comoving projected separation, σ . When calculating this correlation function one assumes that all tracers (usually with no distance information) lie at the known distance of the centre galaxy, given by its redshift (spectroscopic or photometric). In our case this approach keeps the effect of distance measurement errors to a minimum by only using photometric redshifts to estimate comoving distances to the centre galaxies, and to restrict the range of redshifts of tracers (i.e. we never calculate the relative distance between galaxies in the radial direction); this is the main aim behind the choice of this cross-correlation function.

Centre samples comprise galaxies selected by applying the cuts in redshift (spectroscopic or photometric) and absolute magnitude (evaluated at the redshift of each individual galaxy) defined in Section 2. The tracer samples are characterised by the same cuts in rest-frame absolute magnitude (calculated at the redshift of each individual galaxy) and by redshifts $z_{min} - \delta z < z < \min(1.5, z_{max} + \delta z)$, where z_{min} and z_{max} are the limits of the centre sample, and $\delta z = 0.1$. The wider redshift range allowed for tracers results in an increase of the number of pairs around centre galaxies near z_{min} and z_{max} .

The estimator applied in this case is

$$\omega(\sigma) = D_C D_T / D_C R - 1,$$

where $D_C D_T$ and $D_C R$ are counts of pairs of centre vs. tracer, and centre vs. random points, respectively. Random points are extracted from random catalogues created to reproduce the angular geometry of the survey with constant density. Since in the cross-correlation estimator adopted here the tracer sample is positioned at the distance of each centre galaxy, a random catalogue does not need to reproduce a radial selection function.

(ii) We find that the propagation of redshift errors onto magnitude, comoving distance and projected distance estimates, produces systematic effects on our measurements.

We correct for these biases by modifying the projected separations involved in our calculations using a method tested with the mock catalogues.

(iii) We use $\omega(\sigma)$ to estimate the projected correlation function, $\Xi(\sigma)$, following Padilla et al. (2001), Ratcliffe et al. (1998) and Croft, Dalton & Efstathiou (1999). Our interest in the $\Xi(\sigma)$ correlation function lies in that it can be used to obtain the real-space correlation function, our final objective. The functions $\omega(\sigma)$ and $\Xi(\sigma)$ can be related via

$$\omega(\sigma) = B\Xi(\sigma) \quad (3)$$

where the constant B takes into account the selection function, ψ , of the tracer sample and the individual comoving distances to the centre galaxies,

$$B = \frac{\sum_i \psi(y_i^p)}{\sum_i (1/y_i^p) \int_0^\infty \psi(x) x^2 dx}. \quad (4)$$

In this equation, y_i^p is the comoving distance to the i th centre galaxy calculated using its redshift (spectroscopic or photometric), and the integration variable x is comoving distance. In turn, the correlation function $\Xi(\sigma)$ bears a close relationship to the real-space correlation function $\xi(r)$ via

$$\Xi(\sigma) = 2 \int_0^\infty \xi(r = \sqrt{\sigma^2 + \pi^2}) d\pi, \quad (5)$$

where π is the radial component of the 3D separation r .

(iv) For the case of approximating the real-space correlation function by a power law with a slope γ , as $\xi(r) \simeq \left(\frac{r}{r_0}\right)^\gamma$, Equation 5 simplifies to

$$\Xi(\sigma) = r_0^\gamma \left[\frac{\Gamma\left(\frac{1}{2}\right) \Gamma\left(\frac{\gamma-1}{2}\right)}{\Gamma\left(\frac{\gamma}{2}\right)} \right] \sigma^{1-\gamma}, \quad (6)$$

where $\Gamma(x)$ is the Gamma function. We use this relation to calculate the power law correlation length, r_0 , and slope, γ , for each subsample by minimising the quantity

$$\chi^2 = \sum_i \frac{(\Xi^{\text{measured}}(\sigma) - \Xi^{\text{fit}}(\sigma))^2}{\epsilon(\sigma)^2}, \quad (7)$$

where the index i runs over the bins in projected separation σ , $\Xi^{\text{measured}}(\sigma)$ is the measured projected correlation function, $\Xi^{\text{fit}}(\sigma)$ is the estimate from equation 6, and $\epsilon(\sigma)$ is the error in the measured correlation function calculated using the jackknife technique (see Section 5.2).

The method outlined above is a variant of the more common procedure of inverting the real-space correlation function from the angular correlation function $\omega(\theta)$ (where θ is the angular separation between a pair of galaxies) using Limber's equation (Limber, 1954). In our case, however, the use of $\omega(\sigma)$ introduces the use of (i) the distance to centre galaxies which in this work come from photometric redshift estimates and (ii) the redshift distribution of tracers which also comes from photo-zs. This poses the question of whether photometric redshift errors introduce important systematics in our measurements; this is answered in Section 5 where we carry out several tests of the robustness of the method using mock catalogues. It should be stressed that the effect of the photo- z errors would still be similar in an inversion of the angular correlation function using Limber's equation since in this case the photo- z errors would affect the redshift distribution of both, centres and tracers. Our method has

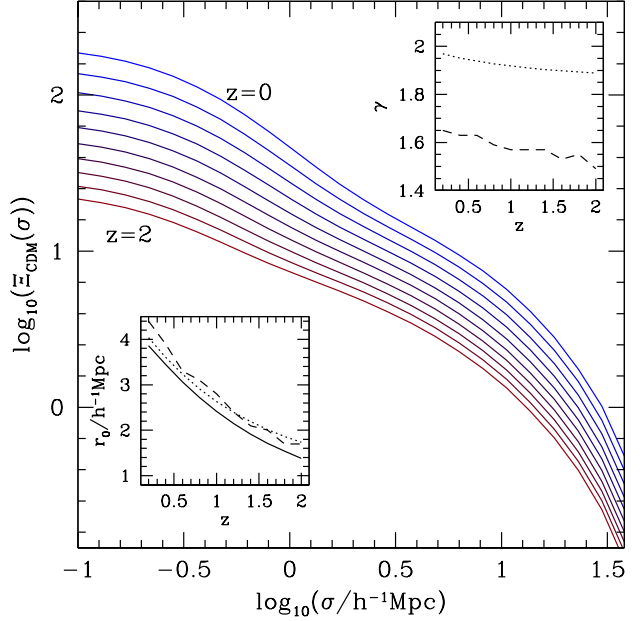


Figure 5. Theoretical projected correlation functions for different redshifts. The insets show the evolution of the correlation length and power law slopes. The solid line shows r_0^{crossing} , dotted lines show $r_0^{\text{rs-fit}}$ and $\gamma^{\text{rs-fit}}$, and dashed lines show the resulting r_0 and γ values from applying our proposed χ^2 method.

the advantage of allowing the use of different redshift ranges for tracers so as to maximise the number of pairs for centre galaxies near the borders of a redshift bin.

4.1 Extracting r_0 from a projected correlation function, $\Xi(\sigma)$.

In this subsection we present an attempt to understand the process of inferring a correlation length r_0 and power law slope γ using a theoretical projected cross-correlation function $\Xi(\sigma)$, paying particular attention at the relation between the parametrisation of this power-law and the physical quantities encoded in the correlation function.

The actual shape of the real-space correlation function deviates from the power law proposed in Section 4 both in predictions from a Λ CDM model (e.g. Zheng et al., 2005) and in observations (e.g. Zehavi et al., 2004). The meaning of r_0 in a power law correlation function is that of the separation at which the correlation function satisfies $\xi(r_0) = 1$. In the case where the shape of $\xi(r)$ is different than a power law, we will use the same equality to define r_0 . With respect to the power law slope γ , notice that its value will depend on the scales used to fit an estimate of a correlation function.

We use theoretical estimates of the real-space and projected correlation functions for the Λ CDM cosmology obtained from non-linear power spectra using the Smith et al. (2003) formalism. For real-space correlations we calculate the value of r_0 in three different ways, (i) searching the separation, r_0^{crossing} , at which $\xi(r_0^{\text{crossing}}) = 1$, (ii) by fitting a power law to the real-space correlation function $\xi(r)$ between separations of $-1 < \log_{10}(r/h^{-1} \text{Mpc}) < 0.3$, in which case we obtain $r_0^{\text{rs-fit}}$; additionally, this procedure also provides an estimate of the power law slope, $\gamma^{\text{rs-fit}}$. (iii) By using the

method described in the third item of the previous section (Eq. 7) of fitting a power law to the projected correlation function between separations of $-1 < \log_{10}(\sigma/h^{-1}\text{Mpc}) < 0.3$ (corresponding to the scales we will use for the measured projected correlation functions). The value of r_0^{crossing} can be considered as the “true” underlying value of r_0 which will not depend on the parametrisation of $\xi(r)$.

Figure 5 shows projected correlation functions for different redshifts (top line for $z = 0$ to bottom line for $z = 2$); the inset on the lower left shows the values of r_0^{crossing} as a solid line (true value), and of $r_0^{\text{rs-fit}}$ as a dotted line; as can be seen both definitions of a correlation length agree to $\sim 0.2h^{-1}\text{Mpc}$ at $z = 0$ and to $\sim 0.4h^{-1}\text{Mpc}$ at $z = 2$. The inset on the upper right shows as a dotted line the resulting values of $\gamma^{\text{rs-fit}}$.

The procedure outlined in item (iii) of Section 4 recovers the correlation length and power law slope, r_0 and γ , shown as dashed lines in the lower left and upper right insets, respectively. This procedure reproduces the process that we will apply to our real data, and therefore can be used to put into context the meaning of the measured values of r_0 and γ in terms of the underlying values r_0^{crossing} and $r_0^{\text{rs-fit}}$ and $\gamma^{\text{rs-fit}}$. As can be seen the recovered correlation length from the projected correlation function following the χ^2 method, is consistent with the direct fit to the real-space correlation function. The power law slope, on the other hand, shows a systematic offset which could be taken into account when analysing the measured projected correlation functions. The origin of this offset comes from the mix of scales characterised by different correlation function slopes, produced by the integral over the radial direction. In this sense, the measured value of γ obtained from $\Xi(\sigma)$ is a different quantity than $\gamma^{\text{rs-fit}}$, the average slope of the real-space correlation function. In our analysis of MUSYC data we will adopt a fixed value for this parameter of $\gamma = -1.8$ roughly consistent with previous estimates for galaxies at similar redshifts and also with theoretical values such as $\gamma^{\text{rs-fit}}$; the statistics only allow one parameter to be obtained from this set of galaxies.

5 TESTS OF THE METHOD

In this section we perform two separate tests of our method. The first is an analysis of possible biases in the estimate of a projected distance using the photometric (instead of spectroscopic) redshifts of centre galaxies; and the second is a test of the recovery of the underlying clustering amplitude using mock catalogues, a process that takes into account the geometry of the MUSYC fields we use, as well as possible problems due to the limited number of galaxies in our subsamples.

5.1 Correcting for biases in the projected separations between centre and tracer galaxies obtained from photometric redshift information

We now test whether the projected separations measured using the photometric redshift of the centre galaxies are comparable to those obtained using the spectroscopic redshifts in the mock catalogues.

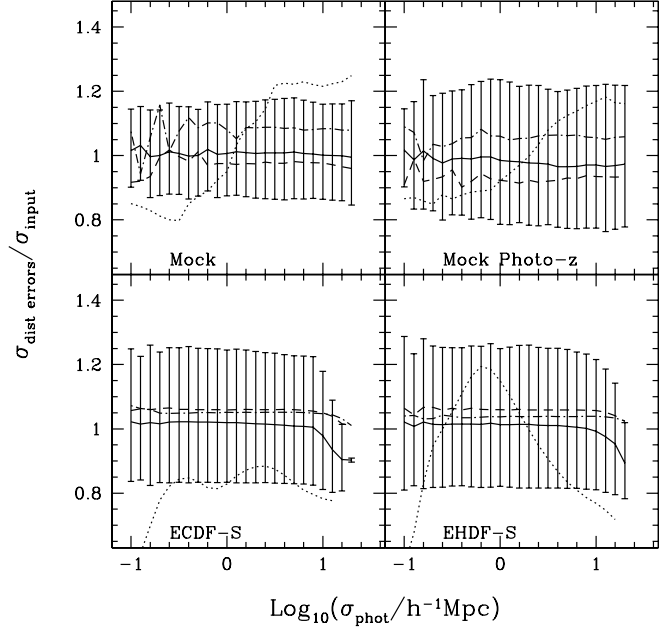


Figure 6. Median (lines) and 10 and 90 percentiles (errorbars) of the distribution of the ratio between projected separations obtained from photometric (or convolved photometric) redshift information to real (or photometric) redshift information as a function of projected separation, for different redshift bins (in dotted, solid, dashed and dot-dashed lines from the lowest to the highest redshift subsamples); percentiles are only shown for the $0.46 < z < 0.68$ sample. Top left: results from the mock catalogues using the estimates of photometric redshifts and the underlying values. Top right: using the photometric redshifts with a further gaussian smearing corresponding to the photo-z uncertainty from Figure 1 against photo-z. The latter procedure can be applied to real data. Lower panels: results for the ECDF-S and EHDF-S MUSYC fields (left and right, respectively) for photometric vs. spectroscopic redshifts where available.

We calculate projected separations using all the galaxies in our subsamples at different redshifts to check for variations with the distance to the observer. In a first approach we use the spectroscopic (true in the case of mock catalogues) and photometric redshifts. The top-left panel of Figure 6 shows the ratio between photometrically and spectroscopically determined projected separations as a function of the projected separation obtained using photometric redshifts. Different line types correspond to different redshift slices (always selected using the photometric redshift estimate). The errorbars indicate the 10 and 90 percentiles of the distribution of ratios in the $0.46 < z < 0.68$ bin. As can be seen, the ratio shows deviations from unity, which are stronger for the lowest redshift subsample, and only marginal for the highest redshifts probed. The large systematic bias at lower redshifts is due to the effect of a $\Delta z \simeq 0.1$ redshift error on a distance of $z \sim 0.2 - 0.4$, which can produce variations in the projected separation of up to a factor of 1.5; at larger distances this becomes almost negligible. Additionally, large-scale structures can produce more important effects on the smaller volume of the lowest redshift samples.

The measurement of the ratio between inferred and underlying projected separations could in principle be used to correct the projected separations obtained from the data,

but would depend on the mock catalogue selected to calculate this bias. We devise an alternative application of this measurement that only uses information available from the observational data, and apply it to the same mock catalogue: we use the measured value of the photometric redshift error (cf. Figure 1, left bottom panel) in the mock, and apply an additional gaussian error of this amplitude to the measured photo-zs. This produces a new version of photo-zs which we will refer to as convolved photo-zs. Then we calculate the projected separations of pairs using the photo-z on the one hand, and convolved photo-z on the other, and show their ratios (convolved photo-z to photo-z) in the upper right panel of Figure 1. As can be seen, these ratios reproduce the results from the original comparison between projected separations obtained from underlying (spectroscopic in the case of real data) and photometric redshifts. Therefore, as this process provides a good estimate of the projected distance bias using only available data from the observations, we can apply it to the MUSYC data. The results for the ECDF-S and EHDF-S fields are shown in the bottom left and right panels of the figure, respectively. Notice that the dispersion around the average values of these ratios are similar for both MUSYC fields. The slightly deeper photometry and infrared coverage in the ECDF-S is responsible for the slightly lower dispersion in the offsets with respect to EHDF-S.

The corrections for the mock and MUSYC fields will be applied to the projected separations before attempting a recovery of the spatial clustering amplitude. As we will show in the following subsection, this bias is the main contributor to an offset in the clustering amplitude when using a projected correlation function and photometric redshift information. Once this is taken into account, the recovery of the clustering from the mock catalogues is similarly successful when using either simulated spectroscopic or simulated photometric redshifts.

5.2 Recovery of the underlying clustering amplitude in mock catalogues

We measure the projected-angular correlation function in the mock subsamples following the method outlined in Section 4 including the correction for the bias present in the measurement of projected separations from using photometric redshifts. We use the measured correlation functions for projected separations in the range $-1 < \log_{10}(\sigma/h^{-1}\text{Mpc}) < 0.3$.

When fitting the projected correlations with the power law model for $\xi(r)$, we encounter a strong degeneracy in the likelihood of the fit as a function of r_0 and γ . We lift this degeneracy by choosing a suitable value for this parameter, $\gamma = -1.8$. As we will show in this section, this choice provides values of r_0 consistent with the underlying values of correlation length.

The mock catalogue constructed using the Baugh et al. (2005) galaxies was extracted from a single $z = 0$ output of the numerical simulation and, as a result, the underlying correlation length does not vary with redshift. However, the model does include a luminosity dependence of clustering, which we calculate directly from the simulation cube. This is shown, as a function of absolute magnitude, as a solid line in the left sub-panels of Figure 7 (the mean redshift of the samples is indicated in each sub-panel; we do not show

the median redshift of each subsample, since these depend slightly on the absolute magnitude limit cuts). As can be seen, this particular model shows a decreasing correlation length as the absolute magnitude decreases (luminosity increases) from $M_r = -18$ to -20.5 , and from then on the clustering increases with the galaxy luminosity³. The right panels show the results for the mock with redshift evolution constructed using Bower et al. (2006) galaxies; the solid line shows the underlying values of the clustering length and its dependence on luminosity and redshift (these galaxies do show the higher clustering for brighter galaxies as in Norberg et al., 2002; they also show a lower clustering amplitude at higher redshifts). In all the panels, the symbols represent the recovered values of r_0 from using the spectroscopic and photometric redshifts in the volume-limited ECDF-S mock samples as solid triangles and open squares, respectively. The right panels also show the recovered correlation lengths for the EHDF-S mock in crosses. Errorbars are calculated using the jackknife technique, applied by constructing 10 subsamples of galaxies from a given mock catalogue (this will also apply to the analysis of the real MUSYC fields) by removing a different 10% of its galaxies for each jackknife subsample. The errorbars are the dispersion with respect to the mean in the results from each jackknife. As can be seen, the recovery of the underlying correlation length is quite successful, regardless of the use of photometric or spectroscopic redshifts (except for the highest redshift samples which start to show slight differences with the underlying clustering specially when using photometric redshifts), indicating that to the level of certainty allowed by sets of data such as the MUSYC fields (limited by sample variance, poisson noise), the bias in the projected distance is the most important factor to take into account in this measurement. These results also indicate that the effect from the width of the distribution in the ratio between measured and true projected distances does not affect the mock results to a detectable degree. It is also noticeable the slightly lower performance shown by EHDF-S mock.

Figure 7 also shows that in the simulation, the variation of the underlying correlation length with luminosity is $\Delta r_0 \sim 1.5h^{-1}\text{Mpc}$ between median $M_r^{r,f} = -21.5$ to -18 , for both mocks. As can be seen, the use of the projected correlation function does allow to detect the underlying dependence of clustering on luminosity with some statistical certainty using samples of galaxies resembling our MUSYC ECDF-S field. The propagation of the photo-z errors into the estimate of the absolute magnitude involved in the sample selection does not appear to play an important role in this result due to the small variation of r_0 with intrinsic luminosity.

We analyse the recovery of the underlying evolution of the clustering amplitude with redshift present in the Bower et al. (2006) galaxy mocks, concentrating on the highest

³ Measurements of this dependence from observational data indicate a steady increase of the clustering length with luminosity (i.e. Norberg et al., 2002, Zehavi et al., 2005) only when the sample of galaxies comprises both blue and red objects. In the case of galaxies from the red-sequence, the dependence of clustering is qualitatively similar to that shown by our mock catalogues (Zehavi et al., 2005, Tegmark et al., 2004; Swanson et al., 2008, Cresswell & Percival, 2009).

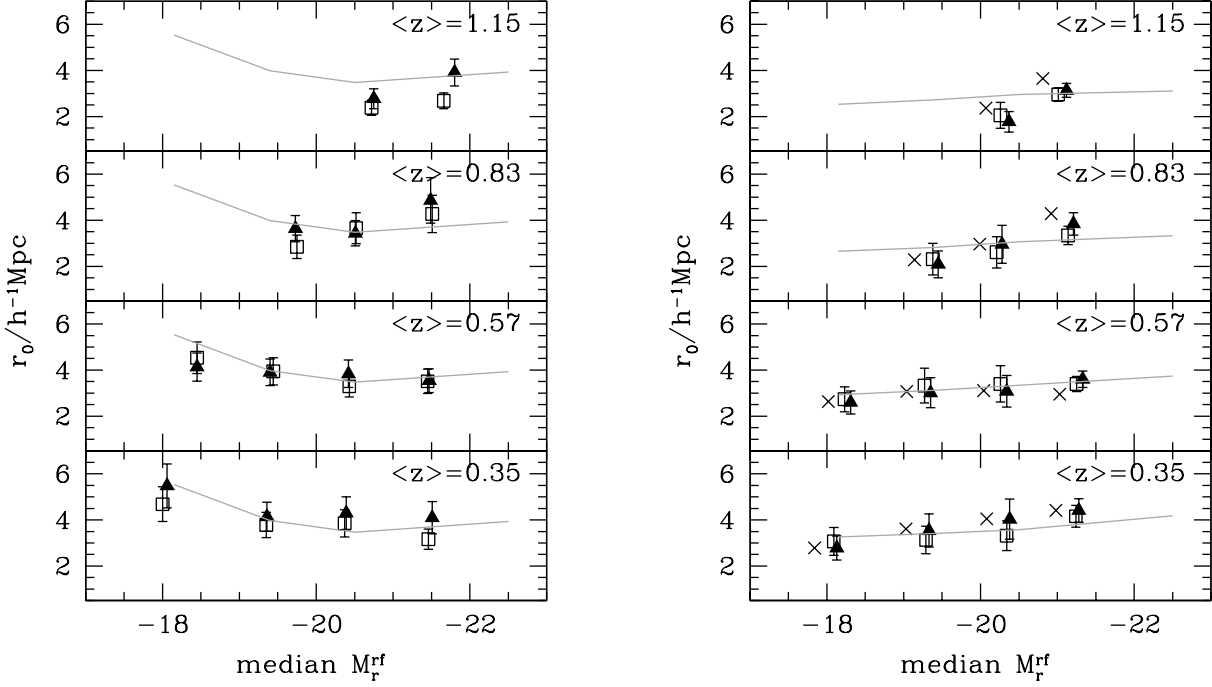


Figure 7. Recovered values of r_0 for two mock ECDF-S catalogues (left panel for Baugh et al., 2005, galaxies, and right panel for Bower et al., 2006, galaxies), using their spectroscopic and photometric redshifts (open squares and filled triangles, respectively). The right panels also show the results for the EHDF-S mock as crosses. Different subpanels correspond to different redshift slices. The solid lines show the underlying clustering amplitude as a function of absolute magnitude in the simulation.

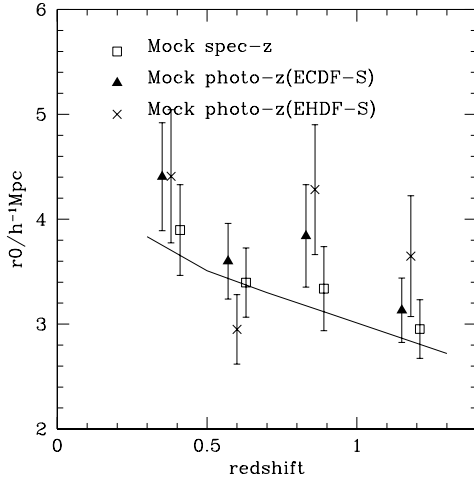


Figure 8. Underlying and recovered dependence of the correlation length with redshift for the mock catalogues constructed using Bower et al. (2006) semi-analytic galaxies; the results are only shown for the $M_r < -21$ sample, when adopting spectroscopic redshift in open squares, ECDF-S photometric redshifts in solid triangles, and EHDF-S (no near infra-red photometry) photometric redshifts in crosses. Errorbars correspond to the jackknife errors in the recovered real-space correlation function.

luminosity subsample. Figure 8 shows as a solid line the underlying dependence of the correlation length with redshift for galaxies with $M_r < 21$ in the simulation; notice that the amplitude of the variation is of $\sim 1 Mpc/h$ in the range of

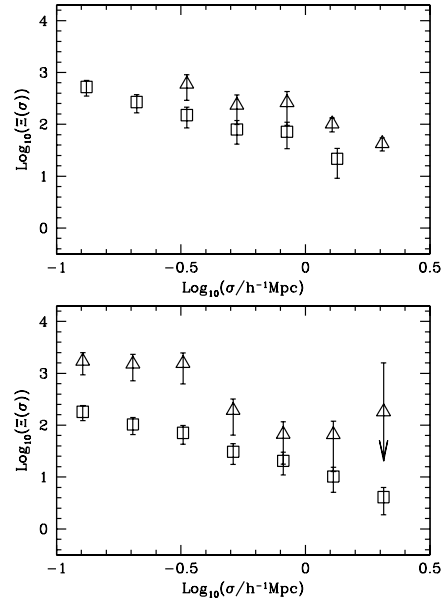


Figure 9. Measured ECDF-S projected correlation functions for galaxies with no restriction on template type (open squares) and for the ETG sample of $M_r(z=0) < -19.7$. Top panel: galaxies with $M_r < -21$ and $0.98 < z_{\text{photo}} < 1.45$. Bottom panel: galaxies with $-20 < M_r < -18.8$ and $0.1 < z_{\text{photo}} < 0.46$. Errorbars are calculated using the jackknife technique.

redshifts $z = 0.3$ to 1.4 . As can be seen, the best agreement with the true evolution is found when using spectroscopic redshifts; it can also be seen that it is not possible to make a highly significant detection of such a small variation with redshift using photometric redshift data (the ECDF-S photometry provides a slightly better match). However, as the results from the mock catalogues do not show systematic differences in the inferred evolution of clustering with redshift in comparison to the true underlying evolution, a detection could be made on observational data characterised by a stronger clustering evolution.

The lack of a perfect match between the measured (from spectroscopic redshifts) and underlying values of clustering amplitude are a consequence of field-to-field variations in the simulation. These should also be expected in the results from the MUSYC fields at a level of $\Delta r_0 \simeq 1h^{-1}\text{Mpc}$ or less, affecting the lowest redshift samples (smallest volumes), preferentially. For example, this variation is consistent with the different average mass of host haloes in the Baugh et al. mock sample with $-18.8 < M_r < -17.5$ and that of all the Baugh et al. galaxies within this magnitude range in the simulation, $\langle M \rangle = 1.6 \times 10^{13}h^{-1}M_\odot$ and $\langle M \rangle = 3 \times 10^{13}h^{-1}M_\odot$, respectively. The amplitude of this effect does not seem to depend on the galaxy luminosity.

We emphasise the fact that our method only uses information readily available in the observational data, and that the photometric redshifts in our mock catalogue are obtained following the same procedure applied to the real data.

6 RESULTS: THE CLUSTERING OF MUSYC GALAXIES

We apply the method outlined in Section 4 to the real data, including the correction of the measured projected separations using the procedure outlined in Section 5.1. Figure 9 shows the resulting projected correlation functions for galaxies with no template type restriction (squares) and ETGs (triangles) with $z > 0.95$ and $M_r < -21$ (top), and $0.1 < z < 0.46$ and $-20 < M_r < -18.8$ (bottom). We use these measurements to infer the correlation lengths, r_0 , using Equation 7. The resulting dependence of the clustering length on median rest-frame r-band absolute magnitude and on the photometric redshift is shown in Figure 10. Results from the EHDF-S and ECDF-S are shown as open squares and solid triangles, respectively; notice that the systematic bias expected for the rest-frame r-band absolute magnitude obtained for EHDF-S should only affect the highest redshift samples and shift the median magnitudes to fainter values by up to ~ 1 mags. The horizontal grey lines show the correlation length of the mass in a ΛCDM cosmology at the mean redshift indicated in each subpanel. The left panel shows the results for the subsamples extracted from the MUSYC EHDF-S and ECDF-S fields, corresponding to different photo- z and M_r ranges described in Section 2. As can be seen, the results from the different fields are not entirely consistent with one another, particularly at low redshift, an indication that field-to-field variations are important due to their relatively small volumes and cosmic variance, as expected from the analysis of the mock catalogues (differences can be larger between the two MUSYC fields than between

measured and underlying r_0 in the mock by up to a factor of ~ 2). It can also be seen that up to $\langle z \rangle = 0.57$, there are hints at a higher clustering for brighter galaxies. Most subsamples of equal luminosity cuts and specially those of ETG galaxies, however, show a systematic tendency to increase their clustering with redshift, as can be seen by comparing the lowest and highest redshift cases for each luminosity range (See Tables 1 and 2 for the resulting values of r_0 for all the explored subsamples). We will come back to this point in the following section. We also notice that samples corresponding to the two lowest redshift ranges show a lower clustering than that expected for the mass (particularly for EHDF-S, and for $M_r^{\text{rf}} > -21$), that is, a bias factor $b < 1$.

The right panel of Figure 10 shows the results for the early type galaxies (notice the change of the scale in the y-axis), selected by a restriction to early-type galaxy templates, and a cut on rest-frame r-band luminosity that depends on redshift so as to take into account the aging of the stellar population of galaxies with no significant star formation activity. This is done using the r-band version of the empirical model adopted by Cimatti et al. (2006), where the brightening of a galaxy luminosity towards higher redshifts (or luminosity dimming as time passes) scales as $\Delta M_r = 0.98 \times z$. It can be clearly seen that we have detected a higher clustering for early type galaxies than for the general population. There is also some evidence for an increase of clustering with redshift (see below) and, for the two lowest redshift bins, of a lower amplitude of clustering for brighter objects in both fields. The latter would represent the first measurement of such an effect at relatively high redshifts. A similar dependence of clustering with luminosity has also been found for red SDSS galaxies in the nearby Universe (Tegmark et al., 2004; Zehavi et al., 2005; Swanson et al., 2008). An analysis of the Baugh et al. semi-analytic galaxy population shows that this can be produced by a large number of faint satellites in high mass DM haloes (clusters of galaxies). This result sheds some light on the similar trend of clustering amplitude with luminosity shown by MUSYC and low redshift early type galaxy samples, which could be due to a large population of intrinsically faint early type galaxies in high-mass concentrations.

Given the possibility that the selection of ETGs using a flux limit on m_R is not complete, we also show the resulting clustering when ETGs are extracted from samples selected in the K-band using $m_K < 22.5$ (open circles, shown only for the brightest ETG samples at each redshift to improve clarity; results for the other subsamples are also in agreement with those shown by the filled triangles). This limit produces samples with similar clustering amplitudes as the selection using R-band fluxes showing that the detection of sources from the deep co-added BVR photometry is able to detect a reasonably complete sample of ETGs at these redshifts. Additionally, the average observer-frame $BVR-K$ colour for our ETG templates in the redshift range $0.3 < z < 1.45$, are reasonably well described (accuracy of 15%) by $(BVR - K)_{\text{ETG-of}} = (1.6 + 2.2 \times z) \pm 0.3$, which at the limiting redshift of our samples $z = 1.45$, translates the $K = 22.5$ limit into $BVR = 27.3 \pm 0.3$, within the range of our detection threshold.

We also test whether a selection of ETGs by colour instead of template types produces significantly different results. In order to do this we find the lower limit in observer-

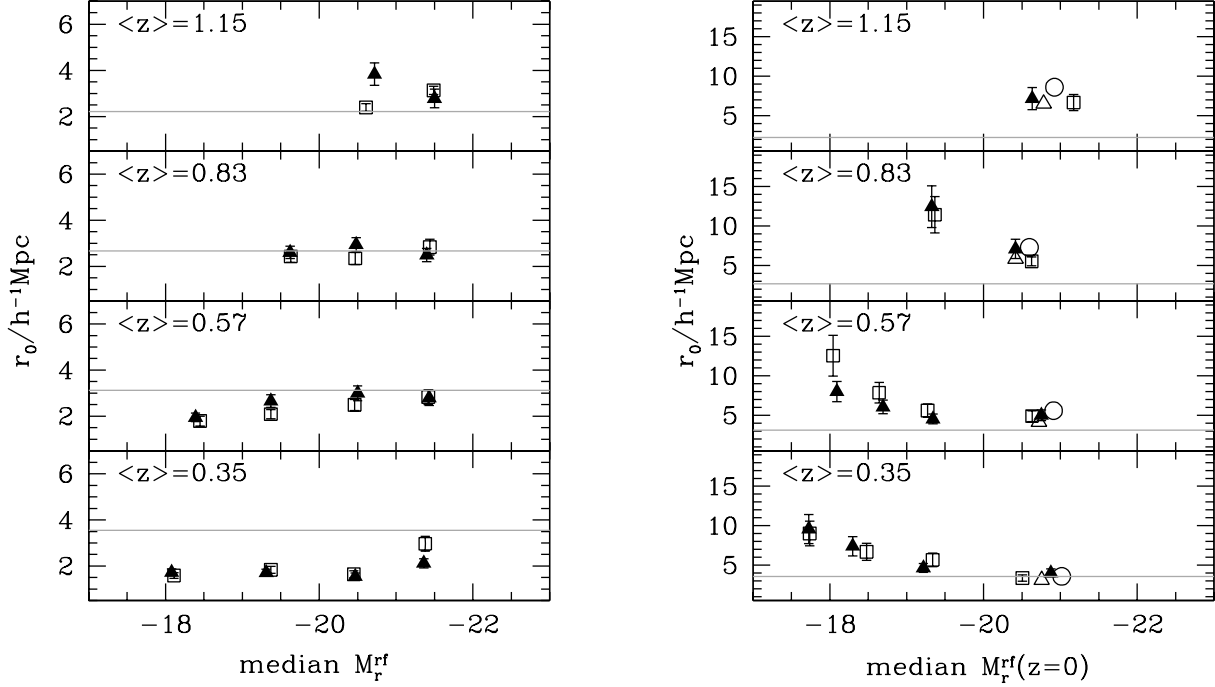


Figure 10. Measured values of r_0 for the ECDF-S and EHDF-S fields (filled triangles and open squares, respectively). The left panel shows the result considering all template types; the right panel shows the results for the early type galaxies, with similar evolved intrinsic luminosities. The right panel also includes the resulting clustering strength of ECDF-S samples selected by applying a lower flux limit in the K-band (open circles) for the brightest samples at each redshift (only shown for the brightest samples in each redshift range, to improve clarity), and the results for ETGs selected as red-sequence galaxies occupying the red branch of the bimodal colour distribution (open triangles). Different subpanels correspond to different redshift slices. The horizontal lines show the expected correlation length for the mass at the redshift of the sample in a Λ CDM model.

Table 1. Resulting correlation lengths r_0 , in units of ($h^{-1}\text{Mpc}$), for the EHDF-S subsamples analysed for galaxies with no restriction on template types (top rows) and for ETGs (bottom rows). As the redshift increases, only the brightest luminosity samples contain galaxies.

All types Abs. Mags.	$0.1 < z < 0.46$	$0.46 < z < 0.68$	$0.68 < z < 0.95$	$0.95 < z < 1.45$
$M_r < -21.0$	3.0 ± 0.3	2.8 ± 0.3	2.8 ± 0.3	3.1 ± 0.2
$-21.0 < M_r < -20.0$	1.6 ± 0.2	2.5 ± 0.2	2.4 ± 0.3	2.4 ± 0.2
$-20.0 < M_r < -18.8$	1.8 ± 0.2	2.1 ± 0.2	2.4 ± 0.3	
$-18.8 < M_r < -17.5$	1.6 ± 0.1	1.8 ± 0.2		
ETG gals.				
$M_r(z=0) < -19.7$	3.4 ± 0.4	4.9 ± 0.7	5.5 ± 0.6	6.5 ± 1.0
$-19.7 < M_r(z=0) < -19.2$	5.7 ± 0.8	5.6 ± 0.8	11.4 ± 2.3	
$-19.2 < M_r(z=0) < -18.2$	6.7 ± 1.1	7.9 ± 1.3		
$-18.2 < M_r(z=0) < -17.0$	9.0 ± 1.6	12.6 ± 2.6		

frame $B - R$ colour that separates blue and red galaxies as a function of redshift. The resulting clustering for the red population (corresponding to the red-sequence) is shown by the open triangles in the right-panel of Figure 10, where as can be seen, there is a good agreement with the results from the selection by template types.

7 DISCUSSION

A global view on the evolution of the clustering of galaxies can be found in Figure 11, where we show the measured values of r_0 as a function of median redshift for the sample of galaxies corresponding to the brightest absolute magnitude cut, $M_r < -21$, when making no distinction on best-fitting template (open symbols), and for the brightest samples of early types alone (small solid symbols). As can be seen, early type galaxies show a higher clustering than

Table 2. Same as Table 1, for the ECDF-S field.

All types Abs. Mags.	$0.1 < z < 0.46$	$0.46 < z < 0.68$	$0.68 < z < 0.95$	$0.95 < z < 1.45$
$M_r < -21.0$	2.1 ± 0.2	2.8 ± 0.3	2.5 ± 0.3	2.8 ± 0.4
$-21.0 < M_r < -20.0$	1.6 ± 0.1	3.0 ± 0.3	2.9 ± 0.3	3.8 ± 0.5
$-20.0 < M_r < -18.8$	1.7 ± 0.2	2.7 ± 0.3	2.6 ± 0.3	
$-18.8 < M_r < -17.5$	1.7 ± 0.2	2.0 ± 0.2		
ETG gals.				
$M_r(z=0) < -19.7$	4.0 ± 0.5	5.0 ± 0.7	7.1 ± 1.2	7.2 ± 1.4
$-19.7 < M_r(z=0) < -19.2$	4.6 ± 0.6	4.5 ± 0.6	12.5 ± 2.6	
$-19.2 < M_r(z=0) < -18.2$	7.4 ± 1.2	6.1 ± 0.9		
$-18.2 < M_r(z=0) < -17.0$	9.6 ± 1.8	8.0 ± 1.3		

the samples with early and late types, and there is a mild trend of an increasing clustering length with redshift for the ETG samples. The samples with no restriction on template types are consistent with roughly constant values of correlation length of $r_0 = (2.6 \pm 0.3)h^{-1}\text{Mpc}$ for the ECDF-S field, and $r_0 = (3.0 \pm 0.4)h^{-1}\text{Mpc}$ for the EHDF-S field, throughout the redshift range considered. For comparison, we show as a dashed line the results from the VVDS survey (Le Fèvre et al., 2005; the dotted lines show the errors), and as a large open circle the results from the DEEP2 survey (Coil et al., 2004). In both cases the results correspond to similar rest-frame luminosities as the MUSYC samples with no restriction on template shown in this figure. As can be seen our results are in very good agreement with these two previous works. We remind the reader that our results also extend the clustering measurements to lower luminosity objects, and that we also add a new measurement of the clustering of early-type galaxies with similar passively evolved luminosities to $z = 0$. Coil et al. (2008) also studied the clustering of DEEP2 galaxies separated according to their rest-frame colours for galaxies at $z \simeq 1$. The solid circle shows the results for their red galaxy sample with equivalent intrinsic luminosities as those characterising our ETG samples. As can be seen our estimates are in agreement with their measurement (particularly the EHDF-S result).

The open stars in Figure 11 show the clustering of SDSS galaxies of different luminosities indicated in black next to each symbol. These clustering results are extracted from Zehavi et al. (2005, they present results up to $L/L^* = 6$), and are extended to higher galaxy luminosities using the fit to the variation of the bias factor by Tegmark et al. (2004). The red labels show the luminosity of early-type galaxies (selected from the red sequence in a colour-magnitude diagram) corresponding to the same clustering amplitude, as measured by Swanson et al. (2008).

The black solid line in Figure 11 corresponds to the evolution of r_0 from the smooth DM density field (calculated using non-linear power spectra from Smith et al., 2003), and the light blue lines show the evolution of the clustering of DM haloes of a given mass (increasing from the lower to the upper lines) as their evolution is followed to $z = 0$ using the merger trees in the numerical simulation⁴. We use these

lines to interpret our clustering measurements. If the results corresponding to galaxies characterised by similar properties (intrinsic luminosity, spectral template) are found to lie on a particular solid light blue line, it could be considered that the lower redshift samples are direct descendants of their higher redshift counterparts. As can be seen, some of our MUSYC subsamples might not be connected in this simple way. In particular, the samples with no restriction on templates, which present narrow errorbars, could allow a statistical refutation of perfect connection of $\sim 5\sigma$ for ECDF-S, $\sim 3\sigma$ for EHDF-S⁵. Luminous galaxies at $z \simeq 1.15$ could evolve into objects with higher clustering than galaxies of similar rest-frame luminosity at $z \simeq 0.37$. The present-day descendants of the bright, volume-limited ECDF-S and EHDF-S subsamples shown here would roughly be within $0.5 < L/L^* < 1.5$. However, the sample of galaxies with no template restriction is not particularly suitable for this analysis since the descendants of many of the galaxies in the high- z samples will probably be below the lower luminosity limit of the low- z samples since we are not taking into account any possible evolution in this case. The selection of ETGs which we analyse next does take into account passive evolution and we are therefore able to analyse their descendants.

For the ETG samples, the refutation of a direct descendant/parent relationship between the $z \simeq 1.15$ and $z \simeq 0.37$ samples is of 2σ and 2.6σ significance for the ECDF-S and EHDF-S, respectively. If this were confirmed with larger galaxy samples, it would conflict with recent exercises where early type galaxies with equivalent evolved $z = 0$ luminosities selected by requiring them to populate the red sequence are compared as descendants/parents of each other. Such attempts have been widely used to study the epoch of assembly of stellar mass in early types (i.e. Cimatti et al., 2006). Given the low SF activity characterising these samples of galaxies, their present-day descendants should also correspond to early type galaxies (unless new SF episodes

tice that the variation in r_0 for the descendants is similar to that of the smooth mass density field. In a plot of the evolution of the bias factor there is a more clear difference between the trends shown by descendants and by the mass; for the latter $b=1$ for all redshifts.

⁵ This of course would still allow some galaxies in one subsample to be descended from those in another.

⁴ This represents the trend of the clustering of descendants; no-

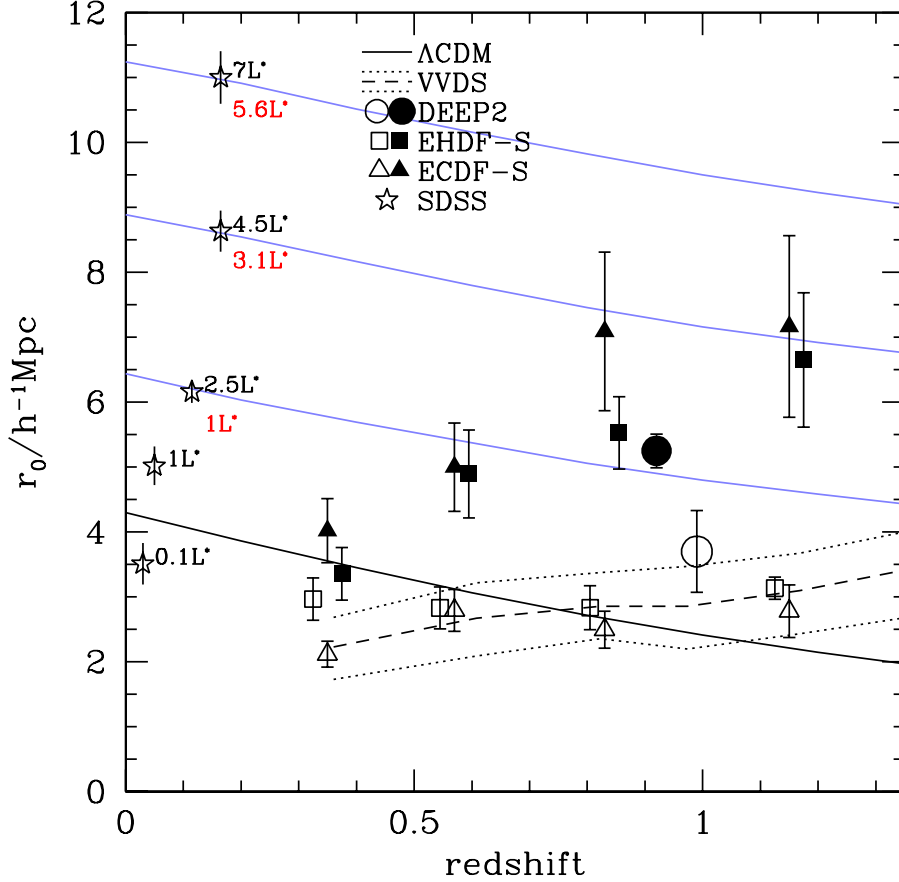


Figure 11. Measured values of r_0 from the projected correlation function measured from bright samples of ECDF-S and EHDF-S (triangles and squares) with no template restrictions (open symbols) and for early types only (small solid symbols); symbols have been slightly displaced along the x-axis to improve clarity. The large open and filled circles show the results from the DEEP2 survey for the full galaxy population (from Coil et al., 2004) and for red galaxies (Coil et al., 2008); the dashed line shows the VVDS results (the dotted lines indicate their $1 - \sigma$ uncertainty). The solid lines show the expected evolution in a Λ CDM universe for the mass (black), and for the descendants of DM haloes of different masses (increasing towards the upper lines, in light blue). The open stars show the clustering length of SDSS galaxies of different luminosities shown in units of L^* in black for the full galaxy population, and in red for early-type galaxies alone.

were triggered). Assuming that this is the case and using the Swanson et al. SDSS $z = 0$ early-type galaxy luminosities (indicated in red labels), we calculate the resulting descendant luminosity of early type galaxies at different redshifts by following the halo descendant tracks that connect the ETG clustering amplitude at redshift z down to $z = 0$ (cf. Figure 11), where we interpolate to find the luminosity of the SDSS ETGs which would be characterised by this clustering amplitude. These results are shown in Figure 12; shaded areas show the uncertainties calculated by propagating the errors in r_0 . As can be seen, the descendant luminosity drops from $L/L^* \sim 2 - 5.2$ to as low as $L/L^* \sim 0.1 - 0.8$ from $z = 1.15$ to $z = 0.37$ (the ranges in L/L^* encompass the results obtained from the EHDF-S and ECDF-S fields). We remind the reader that this result is dependent on the rates of mergers used to trace the descendants of high-redshift galaxy samples; therefore, this conclusion corresponds only to the cosmological model adopted in this paper. We will use these results to study the assembly of massive galaxies in MUSYC in a forthcoming paper (Padilla et al., 2010).

8 CONCLUSIONS

We presented a measurement of the evolution of galaxy clustering with redshift from the MUSYC survey. We used $\sim 50,000$ galaxies in the MUSYC EHDF-S and ECDF-S fields for which photometric redshifts were calculated using a least squares frequentist best-fit method in combination with the synthetic spectra used by the HYPERZ code along with a specially designed template set from Christlein et al. (2009). We divide the sample of galaxies into bins in photo- z delimited by 0.1–0.46, 0.46–0.68, 0.68–0.98 and 0.98–1.45; which results in 4 subsamples with a total number of galaxies ranging between $\sim 9000 - 17000$ each. These are then further divided according to their rest-frame luminosities.

We use a method involving the projected-angular correlation function, which is thoroughly tested using theoretical estimates of the projected correlation function, as well as two mock MUSYC fields. We demonstrate that the application of this technique to samples with photometric redshift

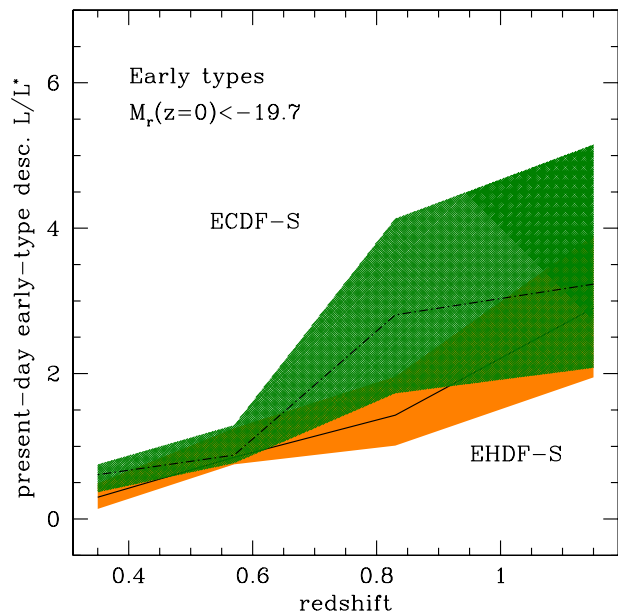


Figure 12. Typical present-day descendant luminosity (L/L^*) for samples of early type galaxies with evolved luminosities $M_r(z=0) < -19.7$, for the EHDF-S and ECDF-S fields (solid and dot-dashed lines, respectively). The shaded areas indicate the uncertainty in the descendant luminosity arising from the uncertainties in the clustering length measurements. Descendants are assumed to be early type galaxies.

information can provide reliable results on the clustering amplitude of galaxies, out to $z \simeq 1.5$.

We find important systematic biases in the determination of projected separations when photometric redshifts are used as an indicator of the distance to a sample of centre galaxies; this effect arises from the important variations introduced in the distance to galaxies by the redshift error, which translates into a change in the projected separation. This bias can be particularly important for low redshift samples, since the relative redshift errors are larger and the small sampled volumes are more sensitive to large-scale structure variations. We propose and test a method to estimate these biases, using only information available from observational data. We find that this is the most important bias affecting the clustering measurement from this method, at least to the degree of certainty allowed by the size of our samples.

The results from MUSYC galaxies indicate that the real-space correlation length r_0 of $M_r < -21$ (rest-frame) galaxies is consistent with constant values over the redshift range explored, $0.1 < z < 1.45$, of $r_0 = (2.6 \pm 0.3)/h^{-1} \text{Mpc}$ and $(3.0 \pm 0.4)/h^{-1} \text{Mpc}$ for the ECDF-S and EHDF-S fields, respectively. These values are consistent within the errorbars with previous estimates from the VVDS survey (Le Fèvre et al. 2005) and DEEP2 (Coil et al., 2004) for samples with similar intrinsic luminosities. By extension, these measurements would also be consistent with the results for the zCOSMOS survey by Meneux et al. (2009) who obtain similar results to the VVDS; a more direct comparison with our measurements would involve replicating their sample selection which we do not attempt at this time.

We also studied the clustering properties of early type

galaxies with similar evolved intrinsic luminosities (using a passive evolution recipe), finding good agreement with a previous measurement of equivalent samples of red galaxies by Coil et al. (2008) at $z \simeq 1$. Samples selected this way at different redshifts have been proposed as tools to study the evolution of the stellar content of early type galaxies with redshift, to infer the typical epoch of assembly. We find indications that such samples may not constitute a single evolving population; furthermore, our results indicate that $z \sim 1$ early type galaxies evolve into present-day objects with a higher clustering than their counterparts of similar evolved luminosity at lower redshifts.

Our results have suffered from considerable cosmic variance (similar to the effects suffered by DEEP2 and VVDS), an issue that will soon be overcome by larger surveys. In particular, the method presented in this paper will be extremely useful to analyse upcoming or planned photometric surveys which will cover areas many orders of magnitude larger than MUSYC. Examples are the Dark Energy Survey (4,000 sq. degrees, Huan et al., 2009), or the Large Synoptic Survey Telescope (20,000 sq. degrees, Ivezić et al., 2008) which, while characterised by photometric redshift errors comparable to those from MUSYC, will allow extremely accurate measurements of the clustering dependence on redshift, luminosity and template type, and in turn on the parent-descendant relation between samples of galaxies at different redshifts.

ACKNOWLEDGMENTS

We acknowledge constructive comments from an anonymous referee. NDP was supported by a Proyecto Fondecyt Regular no. 1071006. This work was supported in part by the “Centro de Astrofísica FONDAP” 15010003, and by BASAL-CATA. This material is based upon work supported by the National Science Foundation under Grant. No. AST-0807570. We are indebted to the Durham group for kindly providing us with GALFORM simulation outputs.

REFERENCES

- Adelberger K. L., Erb D. K., Steidel C. C., Reddy N. A., Pettini M., Shapley A. E., 2005a, *ApJ*, 620, L75.
- Adelberger K. L., Steidel C. C., Pettini M., Shapley A. E., Reddy N. A., Erb D. K., 2005b, *ApJ*, 619, 697.
- Baugh C. M., Lacey C. G., Frenk C. S., Granato G. L., Silva L., Bressan A., Benson A. J., Cole S., 2005, *MNRAS*, 356, 1191.
- Bayarri M.J., Berger J.O., 2004, *STS*, 19, 58.
- Bell E., et al., 2004, *ApJ*, 608, 752.
- Bertin E., Arnouts S., 1996, *A&AS*, 117, 393.
- Bonzonella M., Miralles J.-M., Pelló R., 2000, *A&A*, 363, 476.
- Bower R., Benson A., Malbon R., Helly J., Fenk C., Baugh C., Cole S., Lacey C., 2006, *MNRAS*, 370, 645.
- Brown M., Zheng Z., White M., Dey A., Jannuzi B., Benson A., Brand K., Brodwin M., Croton D.J., 2008, *ApJ*, 682, 937.
- Bruzual G., Charlot S., 2003, *MNRAS*, 344, 1000.
- Bundy K., et al., 2006, *ApJ*, 651, 120.
- Christlein D., Gawiser E., Marchesini D., Padilla N., 2009, *MNRAS*, 400, 429.
- Cimatti A., et al., 2002, *A&A*, 381, L68.
- Cimatti A., et al., 2004, *Nature*, 430, 184.
- Colberg J., et al. 2000, *MNRAS*, 319, 209.

- Colless M., et al. (The 2dFGRS Team), 2001, MNRAS, 328, 1039.
- Coil A., et al., 2004, ApJ, 609, 525.
- Coil A., et al., 2008, ApJ, 672, 153.
- Cooray A., Sheth R., 2002, Phys. Rep., 371, 1.
- Cresswell J., Percival W., 2009, MNRAS, 382, 682.
- Croft R., Dalton G., Efstathiou G., 1999, MNRAS, 305, 547.
- Daddi E., et al., 2005, ApJ, 626, 680.
- di Serego Alighieri S., et al., 2005, A&A, 442, 125.
- Dunkley J., et al. (The WMAP Team), 2009, ApJS, 180, 306.
- Francke, H., et al. (The MUSYC Collab.), 2008, ApJ, 673, 13.
- Gallazzi A., Charlot S., Brinchmann F., White S.D.M., 2006, MNRAS, 370, 1106.
- Gawiser E., et al. (The MUSYC Collab.), 2006, ApJS, 162, 1.
- Gawiser E., et al. (The MUSYC Collab.), 2007, ApJ, 671, 278.
- Glazebrook K., et al., 2004, Nature, 430, 181.
- Gronwall C., et al. (The MUSYC Collab.), 2007, ApJ, 667, 79.
- Guaita L., Gawiser E., Padilla N., Francke H., Bond N., Gronwall C., Ciardullo R., Feldmeier J., Sinawa S., Blanc G., Virani S., 2010, ApJ, 714, 255.
- Hoaglin D.C., Mosteller F., Tukey J., 1983, Wiley Series in Probability and Mathematical Statistics, New York: Wiley, 1983, edited by Hoaglin, David C.; Mosteller, Frederick; Tukey, John W.
- Huan et al. (The Dark Energy Survey Collaboration), 2009, AAS, 21440706.
- Huber M., 2002, PhD Thesis, University of Wyoming.
- Ivezic et al. (The Large Synoptic Survey Telescope Collaboration), arXiv:0805.2366.
- Jing Y.P., Mo H.J., Börner G., 198, ApJ, 494, 1.
- Kovac K., Somerville R. S., Rhoads J. E., Malhotra S., Wang J., 2007, ApJ, 668, 15.
- Lagos C., Cora S., Padilla N., 2008, MNRAS, 388, 587.
- Lagos C., Padilla N., Cora S., 2009, MNRAS Letters, 397, 31.
- Le Fèvre O., et al., 2005, A&A, 439, 877.
- Lee K.-S., Giavalisco M., Gnedin O. Y., Somerville R. S., Ferguson H. C., Dickinson M., Ouchi M., 2006, ApJ, 642, 63.
- Limber D.N., 1954, ApJ, 119, 655.
- Norberg P., et al. (The 2dFGRS Team), 2002, MNRAS, 332, 827.
- Meneux B., et al. (The COSMOS Team), 2009, A&A, 505, 463.
- McCarthy P.-J., et al., 2004, ApJ, 614, L9.
- Ouchi M., et al., 2003, ApJ, 582, 60.
- Ouchi M., et al., 2004, ApJ, 611, 685.
- Padilla N.D., Merchán M.E., Valotto C.A., Lambas D.G., Maia M.A.G., 2001, ApJ, 554, 873.
- Padilla N.D., Baugh C.M., 2002, MNRAS, 329, 431.
- Padilla N.D., Christlein D., Gawiser E., Marchesini D., 2009, in preparation.
- Peacock J.A., Smith R.E., 2000, MNRAS, 318, 1144.
- Pérez-González P., et al., 2008, ApJ, 675, 234.
- Quadri R. et al. 2007, ApJ, 654, 138.
- Ratcliffe A., Shanks T., Parker Q., Fong R., 1998, MNRAS, 296, 173.
- Sánchez A., Baugh C.M., Percival W., Peacock J., Padilla N., Cole S., Frenk C., Norberg P., 2006, MNRAS, 366, 189.
- Saracco P., et al., 2005, MNRAS, 372, L40.
- Seljak U., Warren M., 2004, MNRAS, 355, 129.
- Sheth R., Mo H.J., Tormen G., 2001, MNRAS, 323, 1.
- Smith R., et al., 2003, MNRAS, 341, 1311.
- Sobral D., Best P., Geach J., Smail I., Cirasuolo M., Garn T., Dalton G., Kurk J., 2010, MNRAS, 404, 1551.
- Spergel D.N., et al. (The WMAP Team), 2007, ApJS, 170, 377.
- Swanson M., Tegmark M., Blanton M., Zehavi I., 2008, MNRAS, 385, 1635.
- Tegmark et al. (The SDSS Team), 2004, ApJ, 606, 702.
- Wake D., et al., 2008, MNRAS, 387, 1045.
- White M., Zheng Z., Brown M., Dey A., Jannuzi B., 2007, ApJL, 655, 69.
- York D., et al. (The SDSS Team), 2000, AJ, 120, 1579.
- Zehavi I., et al. (The SDSS Team), 2004, ApJ, 608, 16.
- Zehavi I., et al. (The SDSS Team), 2005, ApJ, 630, 1.
- Zheng Z., et al., 2005, ApJ, 633, 791.
- Zheng Z., Coil A., Zehavi I., 2007, ApJ, 667, 760.